arXiv:cond-mat/0612558v1 [cond-mat.mes-hall] 21 Dec 2006

Gate tunability of stray-field-induced electron spin precession in a GaAs/$In_xGa_{1-x}As$ quantum well below an interdigitated magnetized Fe grating

L. Meier[1,2], G. Salis[1], C. Ellenberger[2], E. Gini[3], and K. Ensslin[2]
[1]*IBM Research, Zurich Research Laboratory, Säumerstrasse 4, 8803 Rüschlikon, Switzerland*
[2]*Solid State Physics Laboratory, ETH Zurich, 8093 Zürich, Switzerland*
[3]*FIRST Center for Micro- and Nanosciences, ETH Zurich, 8093 Zürich, Switzerland*
(Dated: October 05, 2006)

Time-resolved Faraday rotation is used to measure the coherent electron spin precession in a GaAs/$In_xGa(1-x)$As quantum well below an interdigitated magnetized Fe grating. We show that the electron spin precession frequency can be modified by applying a gate voltage of opposite polarity to neighboring bars. A tunability of the precession frequency of 0.5 GHz/V has been observed. Modulating the gate potential with a gigahertz frequency allows the electron spin precession to be controlled on a nanosecond timescale.

PACS numbers:

Considerable effort has been devoted to gaining coherent control over single electron spins in semiconductors, motivated by the potentially long coherence times that make such a two-level system an ideal candidate for a quantum bit [1]. Using pulsed electron spin resonance techniques, Rabi oscillations of single electron spins have been observed in diamond defect centers [2] and in semiconductor quantum dots [3]. Electrical control of the exchange coupling between neighboring spins in quantum dots [4, 5] allows the implementation of two-qubit gate operations. To address individual spins in an array of localized spins, either an ac magnetic field has to be applied locally, or the array has to be exposed to a magnetic-field gradient, whereby individual spins are addressed by changing the frequency of a global ac field. The latter approach might be facilitated by locally tuning the electron g-factor with an electric field [6, 7]. Also, effective ac magnetic fields can be provided locally using electric gates, as has been demonstrated for systems with anisotropic g-factor tensors [8] and for systems with strain-induced spin-orbit coupling [9]. Recently, it has been shown that the magnetic stray field of ferromagnetic structures can be used to manipulate electron spins [10]. This idea has been extended to manipulate single electron spins in a quantum dot [11] via a spatial displacement in the large and inhomogeneous magnetic field. Such a spatial displacement can be induced by applying an electric field to metallic gates, which is technically easier to achieve than providing an ac magnetic field at the high frequencies (GHz) involved.

Here, we report on the control of the electron spin precession in a semiconductor quantum well (QW) using an electric gate voltage and a magnetic stray field. By employing time-resolved Faraday rotation (TRFR) [12], we track the electron spin precession in a QW below an array of ferromagnetic bars made of Fe. In an external magnetic field of sufficient strength to magnetize the Fe bars, the magnetic stray field makes the electron spins precess faster than below an identical grating made out of non-magnetic Au [10]. By applying a gate voltage V_g with opposite sign to neighboring bars of an interdigitated grating, the electron distribution in the QW is moved towards the positively charged bar, and precesses in a higher mean stray field. Application of a voltage of $V_g = \pm 1$ V to a grating with a period of 1 μm leads to an increase in the electron spin precession frequency by up to 0.5 GHz, corresponding to a magnetic field of 70 mT. By modulating the gate voltage with gigahertz frequencies, we achieve control of the electron precession frequency on the nanosecond timescale.

Our sample consists of a 40 nm thick InGaAs QW (8.8% In), sandwiched between the GaAs substrate and a 20 nm GaAs cap layer. Both well and cap are n-doped with Si to ensure long spin lifetimes [13], the latter with a δ-doping in the middle of the layer, the former with a bulk doping aimed at 5 $\times 10^{16}$cm^{-3}. On the surface, arrays of 80 nm thick Fe (Au) bars have been evaporated using electron-beam lithography and standard lift-off processes with a 10 nm Ti adhesion layer between the Fe (Au) and the GaAs surface. The Fe bars were protected from oxidation by 10 nm Al. Neighboring bars have separate electrical connections, so that they can be put on different potentials. We have fabricated interdigitated gratings 100 μm $\times$ 100 μm in size having periods p of 1, 2, and 4 μm and a bar width of half the period.

We use TRFR to trace the electron spin precession in the QW: a circularly polarized picosecond pump pulse from a Ti:Sapphire laser tuned to the absorption edge of the QW ($\lambda = 870$ nm, P = 500 μW) and focused ($\approx$20 μm in diameter) on the grating creates spin-polarized electrons in the conduction band of the QW. The polarization axis of the linearly polarized probe pulse (P = 65 μW, focused on the same spot), which arrives with a time delay Δt on the sample, is rotated by an angle θ proportional to the projection of the spin polarization on the laser beam axis (perpendicularly to the QW). When an external magnetic field is applied in-plane with the QW and perpendicular to the bars, the electron spins precess about the magnetic field axis, resulting in a signal of the form $\theta = \theta_0 \exp(-\Delta t/T_2^*)\cos(2\pi\nu\Delta t)$ with the electron spin precession frequency $\nu = g\mu_B B_{\rm tot}/h$. Here, T_2^* denotes the spin lifetime, g the Landé g-factor, μ_B the Bohr

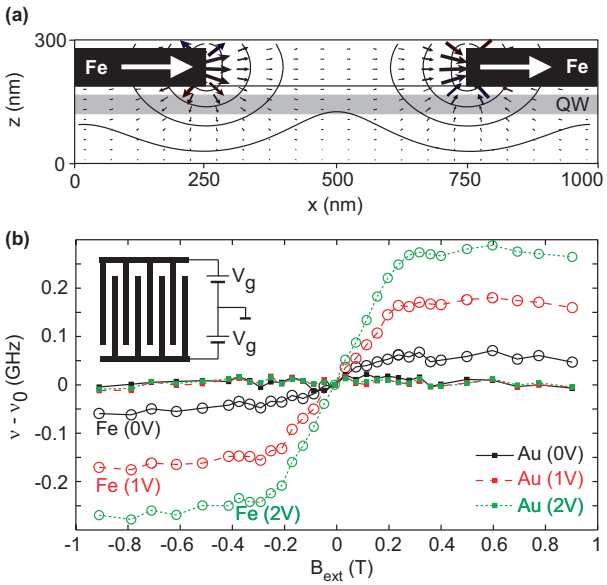


FIG. 1: (Color online) (a) Micro-magnetic simulation of the magnetic stray field of a grating with period 1 μm. The solid lines of constant field indicate magnetic fields of 500, 200, 100, and 50 mT. The QW is shaded gray. (b) Electron precession frequency ν in the QW below the 1 μm grating for different gate voltages. A linear fit $\nu_0 = g\mu_B B_{\rm ext}$ to the data has been subtracted (for Fe the fit only included the saturated region $|B_{\rm ext}| > 0.3$ T). Inset: sketch of a gated interdigitated grating.

magneton and $B_{\rm tot} = B_{\rm ext} + \langle B_{\rm stray}\rangle$ the total magnetic field. Experiments were performed at a temperature of $T = 40$ K where effects of nuclear polarization are below 0.01 GHz [10]. As our laser focus is much larger than the grating period, we measure the electron spin precession averaged over an ensemble of spins that precess in an inhomogeneous magnetic field. This spatial average is determined by the laser field distribution below the grating that acts as an optical mask as well as by the electron distribution within the illuminated regions of the QW. $\langle B_{\rm stray}\rangle$ is the spatially averaged $B_{\rm stray}$ that results from these optical and electronic effects [10].

A numerical simulation of $B_{\rm stray}$ obtained using the micro-magnetic simulation tool OOMMF [14] is shown in Fig. 1(a). The stray field in the center of the QW is expected to be ≈ 200 mT close to a Fe bar and ≈ 50 mT in the middle of the gap. The x-component, which our measurement geometry is most sensitive to, changes sign at the edge of a bar. It is parallel to $B_{\rm ext}$ between the bars and antiparallel below a bar.

Figure 1(b) shows for different V_g the dependence of ν on $B_{\rm ext}$ with a linear background $\nu_0 = g\mu_B B_{\rm ext}$ subtracted ($g_{\rm Au} = 0.5179$, $g_{\rm Fe} = 0.5163$). We first focus on the data for $V_g = 0$ V. While on the sample with the Au grating $\nu - \nu_0$ is constant in $B_{\rm ext}$, $\nu - \nu_0$ on the Fe sample increases linearly up to $|B_{\rm ext}| \approx 0.3$ T. For $|B_{\rm ext}| > 0.3$ T, $\nu - \nu_0$ remains constant at about 0.05 GHz, corresponding to an average stray field of ≈ 7 mT. Magneto-optical Kerr measurements confirm that at this external field, the magnetization of the Fe grating (and with it the stray field) saturates. Simulations assuming a homogeneous electron distribution and illumination between the bars and no illumination below the bars predict $\langle B_{\rm stray}\rangle$ on the order of 100 mT. We ascribe the difference to the probing of negative stray fields antiparallel to $B_{\rm ext}$ below the Fe bars owing to optical diffraction at the grating (as $p \sim \lambda$) and to nonperfect magnetization of the Fe bars due to edge roughness [10].

When applying a voltage of $\pm$ 1 V ($\pm$ 2 V) to neighboring bars, the electrons precess 0.15 GHz (0.25 GHz) faster on the Fe sample than on the Au sample in the saturated region, corresponding to $\langle B_{\rm stray}\rangle = 20$ mT (34 mT). Note that $\nu - \nu_0$ builds up similarly for all voltage traces. In particular it saturates at the same value of $B_{\rm ext}$. This supports that the same stray field is probed with a different spatial averaging for different gate voltages. The spin lifetime T_2^* decreases with an applied gate voltage, also indicating a change in spatial averaging. However, the situation is more complicated, since the gate voltage increases the non-radiative recombination rate as seen in a time-resolved photoluminescence experiment (data not shown).

In Fig. 2, $B_{\rm ext}$ has been set to 1.05 T, where the magnetization of the Fe bars is saturated. Figure 2(a) shows $\nu(V_g)$ for Fe and Au gratings and three different periods. In samples with Au gratings, ν changes little with V_g in contrast to samples with Fe gratings, where ν increases by a few tenths of a gigahertz as $|V_g|$ is increased. We ascribe the small differences in $\nu_{\rm Au}$ at $V_g = 0$ V for $p = 1, 2$, and 4 μm to small variations in g due to strain from the grating. Fits yield $g_{Au}^{1,2,4\mu{\rm m}} = 0.5211, 0.5225$, and 0.5253.

In Fe samples, the increase in ν with V_g is more pronounced for gratings with smaller p, whereas the stray-field effect on ν at $V_g = 0$ is larger for gratings with large p. The understanding of this observation is facilitated by investigating a mixed Fe/Au grating, in which every other Fe bar has been replaced by a Au bar. As long as a positive V_g is applied to the Au bars, $\nu(V_g)$ obtained is similar to $\nu(V_g)$ of the pure Fe sample, see Fig. 2(b). However, a negative voltage applied to the Au bars leads to a *decrease* of ν on the mixed Fe/Au sample below the value on the reference Au sample, indicating that the stray field effectively reduces $B_{\rm tot}$.

TRFR relies on the circular birefringence at the absorption edge of the QW. Spin polarization leads to different Fermi energies for spin-up and spin-down electrons $E_F^{\uparrow,\downarrow}$. The electron density in our QW is on the order of 10^{16} m^{-2}. With an estimated absorption of 1% in the QW, the spin polarization in the conduction band is around 5% and $|E_F^{\uparrow} - E_F^{\downarrow}| \approx 0.05 E_F$ (≈ 2 meV). TRFR therefore only probes electrons close to the (mean) Fermi energy E_F.

A positively charged bar leads to an accumulation of electrons below the bar, but since TRFR only measures electrons close to E_F, the resulting higher electron density does not enhance the TRFR signal. However, when a bar is negatively charged and all electrons are depleted

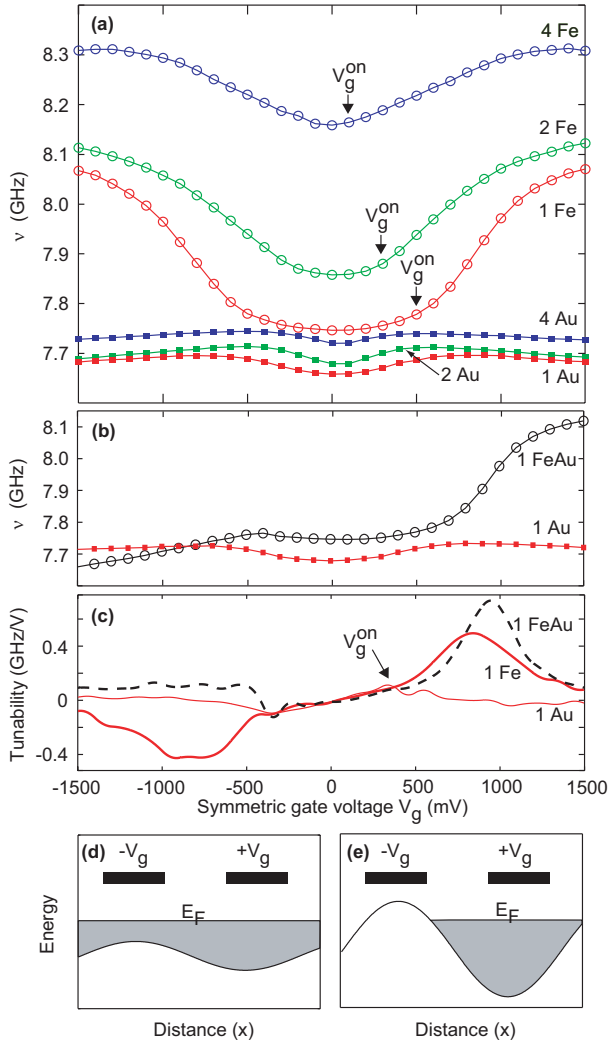


FIG. 2: (Color online) (a) Electron precession frequency ν at $B_{\rm ext} = 1.05$ T as a function of V_g. (b) $\nu(V_g)$ for a Au and a mixed Fe/Au grating (V_g is applied to the Au bars, $-V_g$ to the Fe bars). (c) Gate tunability of the electron precession frequency $\partial\nu/\partial V_g$ as a function of V_g. (d) and (e) Schematic conduction band modulation and Fermi energy E_F in the QW for (d) a small and (e) a large gate voltage V_g.

from below the bar, then no electrons from this region will contribute anymore to the TRFR signal and to the averaged ν [see Fig. 2(d) and (e)].

The smaller the grating period p, the larger the diffraction that leads to a probing of negative stray fields below a Fe bar, resulting in a smaller ν. Besides optical diffraction, effects of surface-plasmon-enhanced transmission [15, 16] through the metallic gratings might also possibly play a role in the illumination of the QW below a bar. Applying $\pm V_g$ to a pair of neighboring bars has no effect on the bar at $+V_g$, but removes contributions from electron spins in the negative stray field below the bar at $-V_g$, which results in an overall increase of ν. The larger the illuminated region below a bar (i.e., for small p), the larger the increase in ν when this region is depleted below the negatively charged bar.

Let us now return to the pure Fe grating. The increase in ν is not linear in V_g. The sensitivity $\partial\nu/\partial V_g$ of ν to changes in V_g for the $p = 1$ μm grating is plotted in Fig. 2(c). For $V_g < V_g^{\rm on} \approx 500$ mV the increase is small and very similar for both the Fe and the Au (as well as the mixed Fe/Au) grating. We suspect that in this regime, ν changes because of a variation of the electron g-factor by about 0.001. Possible explanations for such an electric-field-induced modification of spin dynamics include changes in the overlap between electron and hole wavefunctions [17], band-structure effects [18, 19], and strain-induced spin-orbit effects [20]. When probing a single 2 μm wide gap between two large, electrically contacted Fe (Au) gates (data not shown), we find a very similar behavior in $\nu(V_g)$ as in the case of the Fe (Au) grating with $p = 4$ μm (i.e., 2 μm bar and 2 μm gap). Hence, measuring a grating is equivalent to measuring a single gap, but the grating enhances the signal-to-noise ratio considerably. Specifically, in both cases, the sign of the x-component of the electric field is not of importance: in a single gap the electric field always points in one direction, whereas on a grating, we average over fields pointing in the x- and in the $-x$-direction.

For $|V_g| > V_g^{\rm on}$, ν increases strongly on the 1 μm Fe sample, whereas it remains constant on the 1 μm Au sample. The tunability is highest around $V_g \approx 800$ mV, where a change of 1 V in V_g leads to a variation of about 0.5 GHz in ν, corresponding to an effective stray field of $\approx$ 70 mT.

The on-set voltage $V_g^{\rm on}$ is smaller for larger p. A straightforward analysis of the electric field between and below the bars can explain this dependence on V_g. As mentioned above, the relevant mechanism that increases ν is the depletion of the QW below the negatively charged gate. In the center below a bar, far away from an edge, vertical electric fields dominate. With a capacitor model, we estimate the potential drop between gate and QW needed to deplete the QW to be roughly 100 mV, which is lower than $V_g^{\rm on}$. For voltages which are more negative than required for the depletion of the electron gas, lateral electric fields between the bars become important, similar to the situation in quantum point contacts [21].

Close to the edge of a bar, where the magnetic stray fields are highest, however, lateral electric fields dominate. Under illumination at $V_g = 1$ V, a considerable current of approximately 1 μA is measured through a gated grating, yielding an estimated resistance of 2 MΩ. This resistance can be seen as a series of three resistances: a forward-biased Schottky barrier R_s^f from one bar to the QW, the resistance $R_{\rm QW}$ of the QW itself, and a reverse-biased Schottky barrier R_s^r from the QW to the other bar. The period $p = d_{gate} + d_{gap}$ is the sum of the gate and the gap width. The (lateral) electric field in the QW

is

$$E_{\rm QW} = \frac{V_{\rm QW}}{d_{\rm gap}} = \frac{R_{\rm QW}}{d_{\rm gap}} \frac{2V_g}{R_s^f + R_s^b + R_{\rm QW}} \approx \frac{V_g}{d_{\rm gap}} \frac{R_{\rm QW}}{R_s^f + R_s^b},$$

where we have assumed $R_s^b \gg R_{\rm QW}$. Enlarging the channel length $d_{\rm gap}$ increases its resistance, i.e. $R_{\rm QW} \propto d_{\rm gap}$, whereas enlarging $d_{\rm gate}$ reduces the resistance of the Schottky contact, as the area between gate and the sample surface is increased, thus $R_s^{f,b} \propto 1/d_{\rm gate}$. As a consequence, $E_{\rm QW} \propto d_{\rm gate} V_g$.

We assume that a critical (lateral) field $E_{\rm QW}^{\rm on}$ is needed to significantly shift the depletion edge of the electron gas close to the bar edge and to move the electrons toward the positively charged bar. Then, for larger $d_{\rm gate}$ the onset voltage decreases:

$$V_g^{\rm on} \propto E_{\rm QW}^{\rm on}/d_{\rm gate}. \quad (1)$$

This qualitatively explains the dependence of $V_g^{\rm on}$ on the grating geometry. In addition, we experimentally tested relation (1) by fabricating gratings with $d_{\rm gap} = a d_{\rm gate}$, a = 1, 2, and 3. Changing $d_{\rm gap}$ did not significantly alter $V_g^{\rm on}$, whereas a larger $d_{\rm gate}$ reduced $V_g^{\rm on}$ substantially.

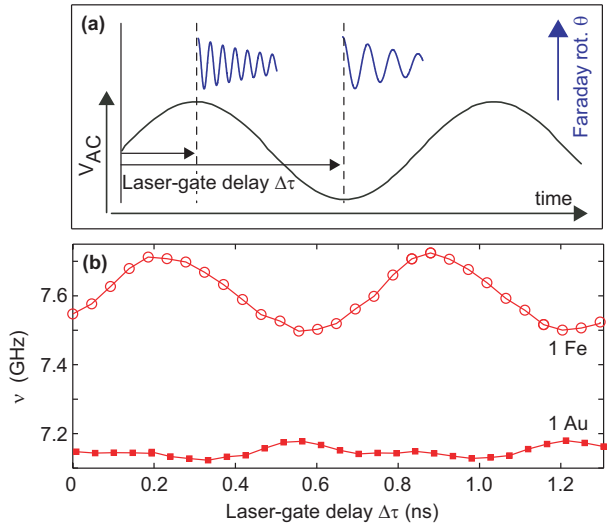


FIG. 3: (Color online) (a) Measurement of the electron spin precession at different phase shifts between laser and ac voltage (see text for details). (b) Electron precession frequency ν as a function of the phase shift between laser pulse and ac voltage phase.

In Fig. 3 we present results with a high-frequency-modulated gate voltage on the $p = 1$ μm grating. While all odd bars are put on ground potential, we apply $V_{\rm dc} = -2$ V [corresponding to $V_g = -1$ V in Fig. 2(a)] to the even bars and add a modulation $V_{\rm ac}(t) = V_{\rm ac}^0 \sin(2\pi f t)$, with $f = 1.44$ GHz. An RF power of 10 dBm was used, corresponding to a $V_{\rm ac}^0$ of about 0.7 V. Figure 3(a) explains the measurement principle: by scanning the phase difference between the laser pulse and the ac modulation $\Delta\tau$, we are able to track the electron spin precession at different phases of the ac modulation.

Figure 3(b) shows ν as a function of $\Delta\tau$. Whereas on the Au sample ν oscillates only weakly with $\Delta\tau$, ν exhibits a strong periodic behavior with a period of $1/f$ and an amplitude ν_1 of about 0.1 GHz on the Fe sample. This is explained by assuming that the electrons in the QW follow the ac modulation. When $\Delta\tau$ is such that the laser pulse coincides with a minimum in $V_{\rm ac}$, then the voltage below the even bars is negative most of the time we measure the electron spin precession, depleting the electrons in the QW below and, as explained for the dc case above, ν is maximal. A similar argument explains the minima in ν. For experimental reasons, we cannot quote $\Delta\tau$ in absolute numbers, we measure only the relative change.

A quantitative estimate for the oscillation amplitude ν_1 can be obtained from the derivative of $\nu(V_g)$, given in Fig. 2(c). Taking into account that only one gate is modulated, we estimate

$$\nu_1 = \frac{1}{2} \left.\frac{\partial \nu}{\partial V_g}\right|_{V_g = -1\ \rm V} V_{\rm ac}^0 \approx 0.18\ \rm GHz,$$

which is in reasonable agreement with our measurement. To prevent the effects of $V_{\rm ac}(t)$ on ν from being averaged out, we extract ν only from a few oscillations during the first $T_{\rm fit} = 400$ ps of the spin precession (shorter than the ac period $T_{\rm ac} = 1/f \approx 700$ ps). Since a few (≈ 3) electron spin oscillations are needed to determine ν with ample precision, we cannot fulfill the ideal case of $T_{\rm fit} \ll T_{\rm ac}$, leading to some reduction of the observed oscillation amplitude of ν. At lower frequencies on the order of several 100 MHz, we have measured an oscillating $\nu(\Delta\tau)$ also on the Au sample that cannot be explained by a magnetic stray field and will be subject of further investigations.

In conclusion, we have observed a tunability of the electron spin precession below a magnetized Fe grating. By applying a gate voltage to an interdigitated grating, we are able to tune the electron spin precession frequency by 0.5 GHz/V, corresponding to an effective magnetic stray field of about 70 mT/V. Modulating the gate potential with a frequency of 1.44 GHz enables the electron spin precession to be controlled on a nanosecond timescale. This could be useful for further experiments that address electron spin resonance using magnetic stray fields.

We thank O. Homan for help with sample preparation, M. Tschudy for the evaporation of Fe, and R. Allenspach and T. Ihn for fruitful discussions.

[1] D. Loss and D. P. DiVincenzo, Phys. Rev. A **57**, 120 (1998).

[2] F. Jelezko, T. Gaebel, I. Popa, A. Gruber, and J. Wrachtrup, Phys. Rev. Lett. **92**, 076401 (2004).

[3] F. H. L. Koppens, C. Buizert, K. J. Tielrooij, I. T. Vink, K. C. Nowack, T. Meunier, L. P. Kouwenhoven, and L. M. K. Vandersypen, Nature **442**, 766 (2006).

[4] J. R. Petta, A. C. Johnson, J. M. Taylor, E. A. Laird, A. Yacoby, M. D. Lukin, C. M. Marcus, M. P. Hanson, and A. C. Gossard, Science **309**, 2180 (2005).

[5] F. H. L. Koppens, J. A. Folk, J. M. Elzerman, R. Hanson, L. H. W. van Beveren, I. T. Vink, H. P. Tranitz, W. Wegscheider, L. P. Kouwenhoven, and L. M. K. Vandersypen, Science **309**, 1346 (2005).

[6] H. W. Jiang and E. Yablonovitch, Phys. Rev. B **64**, R41307 (2001).

[7] G. Salis, Y. Kato, K. Ensslin, D. C. Driscoll, A. C. Gossard, and D. D. Awschalom, Nature **414**, 619 (2001).

[8] Y. Kato, R. C. Myers, D. C. Driscoll, A. C. Gossard, J. Levy, and D. D. Awschalom, Science **299**, 1201 (2003).

[9] Y. Kato, R. C. Myers, A. C. Gossard, and D. D. Awschalom, Nature **427**, 50 (2004).

[10] L. Meier, G. Salis, C. Ellenberger, K. Ensslin, and E. Gini, Applied Physics Letters **88**, 172501 (2006).

[11] Y. Tokura, W. G. van der Wiel, T. Obata, and S. Tarucha, Phys. Rev. Lett. **96**, 047202 (2006).

[12] S. A. Crooker, D. D. Awschalom, and N. Samarth, Selected Topics in Quantum Electronics, IEEE Journal of **1**, 1082 (1995).

[13] J. M. Kikkawa and D. D. Awschalom, Phys. Rev. Lett. **80**, 4313 (1998).

[14] `http://math.nist.gov/oommf/`

[15] T. W. Ebbesen, H. T. Lezec, H. F. Ghaemi, T. Thio, and P. A. Wolff, Nature **391**, 667 (1998).

[16] U. Schröter and D. Heitmann, Phys. Rev. B **58**, 15419 (1998).

[17] I. Y. Gerlovin, Y. K. Dolgikh, S. A. Eliseev, V. V. Ovsyankin, Y. P. Efimov, I. V. Ignatiev, V. V. Petrov, S. Y. Verbin, and Y. Masumoto, Phys. Rev. B **69**, 035329 (2004).

[18] F. A. Baron, A. A. Kiselev, H. D. Robinson, K. W. Kim, K. L. Wang, and E. Yablonovitch, Phys. Rev. B **68**, 195306 (2003).

[19] E. L. Ivchenko, A. A. Kiselev, and M. Willander, Solid State Comm. **102**, 375 (1997).

[20] A. Malinowski, R. S. Britton, T. Grevatt, R. T. Harley, D. A. Ritchie, and M. Y. Simmons, Phys. Rev. B **62**, 13034 (2000).

[21] B. J. van Wees, H. van Houten, C. W. J. Beenakker, J. G. Williamson, L. P. Kouwenhoven, D. van der Marel, and C. T. Foxon, Phys. Rev. Lett. **60**, 848 (1988).